Probe-diverse Ptychography

I. Peterson[1], **R. Harder**[2], **I.K. Robinson**[3,4]

[1]*ARC Centre of Excellence for Coherent X-ray Science, the University of Melbourne, School of Physics, Victoria, 3010, Australia*
[2]*Advanced Photon Source, Argonne National Laboratory, Argonne, IL 60439, USA*
[3]*Research Complex at Harwell, Didcot, Oxfordshire OX11 0DE, UK*
[4]*London Centre for Nanotechnology, University College London, London, WC1H 0AH, UK*
[*]*Corresponding author: isaacrp@unimelb.edu.au*

Abstract: An extension of ptychography is proposed that can use diffraction data obtained by scanning a sample through multiple probes with distinct amplitude and phase profiles to iteratively retrieve high-resolution images of the sample and all probes simultaneously. The method is shown to yield improvements in the reconstructed sample image compared to those obtained using the standard, single-probe ptychographic configuration.

OCIS codes: (340.7440) X-ray imaging; (340.7460) X-ray microscopy.

References and links

1. J.M. Rodenburg and H.M.L Faulkner, App. Phys. Lett., 85, 20, (2009)
2. A. M. Maiden, J. M. Rodenburg, Ultramicroscopy, 109, 1256-1262 (2009).
3. P. Thibault, M. Dierolf, A. Menzel, O. Bunk, C. David and F. Pfeiffer, Science **321** 379, (2008)
4. O. Bunk, M. Dierolf, S. Kynde, I. Johnson, O. Marti and F. Pfeiffer, Ultramicroscopy, 108, 481487 (2008).
5. M. Dierolf, A. Menzel, T. Thibault, P. Schneider, C.M. Kewish, R. Wepf, O. Bunk, and F. Pfeiffer, Nature **467**, 436 (2010).
6. J. M. Rodenburg, A. C. Hurst, A. G. Cullis, B. R. Dobson, F. Pfeiffer, O. Bunk, C. David, K. Jefimovs, and I. Johnson, Phys. Rev. Lett. 98, 034801 (2007).
7. C.T. Putkunz, A.J. DAlfonso, A.J. Morgan, M. Weyland, C. Dwyer, L. Bourgeois, J. Etheridge, A. Roberts, R.E. Scholten, K.A. Nugent, L.J. Allen, Phys. Rev. Lett. 108, 073901 (2012).
8. M. J. Humphry, B. Kraus, A.C. Hurst, A. M. Maiden, J.M. Rodenburg, Nat. Commun. 3, 9-13 (2012).
9. A.J. D'Alfonso, A.J. Morgan, A.W.C. Yan, P. Wang, H. Sawada, A.I. Kirkland, and L.J. Allen, Physical Review B, 89, 064101 (2014).
10. X. Huang, M. Wojcik, N. Burdet, I. Peterson, G. Morrison, D. Vine, D. Legnini, R. Harder, Y. Chu, I. Robinson, Opt. Express, 20, 24038-24048 (2012)
11. P. Thibault, M. Dierolf, O. Bunk, A. Menzel, and F. Pfeiffer, Ultramicroscopy 109, 338343 (2009).
12. B.L. Henke, E.M. Gullikson and J.C. Davis, Atomic Data and Nuclear Data Tables, 54, 181-342 (1993)
13. J. Miao, and D. Sayre, Acta Crystallographica Section A: Foundations of Crystallography, 56, 596–605,(2000).

1. Introduction

Ptychography, in its modern iterative form [1, 2, 3], is an extension of Coherent Diffractive Imaging (CDI) that promises to deliver atom-scale imaging of extended samples without the restrictions imposed by an objective lens. A ptychographic diffraction dataset is obtained by translating the sample through a localised, coherent probe in steps small enough to ensure that the illuminated sample regions are sufficiently overlapped [4]. The dataset is used with iterative phase retrieval algorithms to recover high-resolution, quantitative images of the probe and sample over an extended field of view. Overlapping the illuminated sample regions provides a high level of redundancy in the ptychographic dataset and can significantly improve the accuracy and robustness in the sample image retrieval compared to standard CDI. As a consequence,

there has been significant interest in using ptychographic CDI with an X-ray probe [3, 5, 6], and more recently using an electron probe [7, 8, 9].

Although overlapping the illuminated sample regions of the sample can assist in the sample image retrieval, the image retrieval algorithms can become trapped, resulting in sample image artefacts or the complete failure in algorithm convergence. These stagnation points can be a particular problem in the presence of noise, deviations from perfect spatial or temporal coherence and errors in the recorded ptychographic scan trajectory.

In this paper a method is proposed that scans the target sample through a number of distinct probes with varying amplitude and phase profiles. The resulting probe-diverse ptychographic dataset is used in conjunction with a modified version of the ePIE algorithm [2] to retrieve high-resolution, quantitative images of the sample and all illuminating probes simultaneously. It is shown that this method can yield significant improvements in the reconstructed sample image compared to those obtained using the standard single-probe ptychographic phase-retrieval scheme.

2. Method

The proposed "probe-diverse" ptychographic algorithm can use ptychographic data generated from N distinct probes, $\{P_1(\mathbf{r}),...,P_N(\mathbf{r})\}$, on a target sample with sample transmission function, $O(\mathbf{r})$, where $\mathbf{r}$ is a co-ordinate vector in the sample plane. The sample is scanned through each probe over N associated scanning trajectories, $\{\mathbf{s}_1,...,\mathbf{s}_N\}$. With the sample at the j^{th} scan position of the n^{th} scanning trajectory, $\mathbf{s}_{n,j}$, the exit surface wave, $\psi_{n,j}(\mathbf{r})$, is given by

$$\psi_{n,j}(\mathbf{r}) = O(\mathbf{r}-\mathbf{s}_{n,j})P_n(\mathbf{r}).$$

The far-field wavefield $\Psi_{n,j}(\mathbf{k})$, where $\mathbf{k}$ is a far-field co-ordinate vector, is obtained by the Fourier relationship, $\Psi_{n,j}(\mathbf{k}) \propto \mathbb{F}[\psi_{n,j}(\mathbf{r})]$, where $\mathbb{F}$ is the two-dimensional Fourier transform. An updated estimate of $\Psi_{n,j}(\mathbf{k})$ is obtained by enforcing consistency with the recorded diffraction data, $I_{n,j}(\mathbf{k})$, via the modulus constraint, defined as

$$\Psi'_{n,j}(\mathbf{k}) = \Psi_{n,j}(\mathbf{k})\frac{\sqrt{I_{n,j}(\mathbf{k})}}{|\Psi_{n,j}(\mathbf{k})|}. \tag{1}$$

The accuracy of the current wavefield estimate can be measured using the χ^2 metric, where

$$\chi^2_{n,j} = \frac{\sum_{\mathbf{k}}\left[|\Psi_{n,j}(\mathbf{k})| - \sqrt{I_{n,j}(\mathbf{k})}\right]^2}{\sum_{\mathbf{k}} I_{n,j}(\mathbf{k})}. \tag{2}$$

The updated wavefield, $\Psi'_{n,j}(\mathbf{k})$, is then propagated back to the sample plane where the sample transmission, $O(\mathbf{r})$, and the n^{th} probe, $P_n(\mathbf{r})$, are updated according to the overlap constraint suggested by Maiden *et al.* [2]. The algorithm cycles through all probes and all scanning trajectories, enforcing consistency with the probe-diverse diffraction dataset. The iterative application of the above steps enables the recovery of the sample image and all illuminating probes simultaneously.

3. Experiment

The algorithm was tested using X-ray data obtained at the Advanced Photon Source (APS) beamline 34-ID-C using an experimental geometry detailed elsewhere [10]. All measurements were conducted at an X-ray energy of 9 keV ($\lambda = 0.138$ nm). A horizontal coherence-defining slit set to 102.7μm wide, and located 26 m from the undulator, was used as a secondary source.

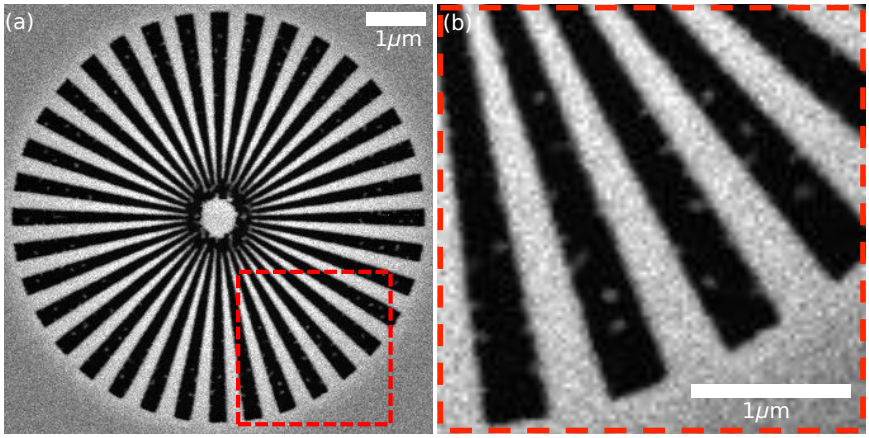

Fig. 1. (a) A SEM image of the star shaped aperture lithographed into a tungsten layer. Errors in the lithography resulted in a series of tungsten deposits on the star spokes, seen as small ($\sim$ 100 nm) "spots" in the closeup in (b).

A set of beam defining slits, located approximately 48 m downstream from the undulator and within the 34-ID-C experimental hutch were used to vary the phase and amplitude profile of the incident illumination. The beam-defining slits were initially set to widths of 10 μm $\times$ 20 μm in the horizontal and vertical directions respectively. The resulting probe was focussed onto the target sample using a set of Kirkpatrick-Baez (KB) mirrors. The vertical and horizontal focussing mirrors were 0.22 m and 0.12 m upstream of the sample stage respectively, with the angle of incidence set to approximately 3 milliradians relative to the beam. The sample (shown in Fig. 1) was manufactured by depositing a 1.5 μm thick tungsten layer onto a silicon nitride support membrane. A series of star shaped apertures were lithographed into the tungsten layer. Errors in the manufacture resulted in small ($\sim$ 100 nm) tungsten remnants on the star spokes, seen as "spots" in the closeup in Fig. 1 (b). At 9 keV the sample attenuated 70% of the beam [12], with full transmission through the lithographed regions.

The star shaped aperture was scanned through the probe using an *xyz* nPoint NPXY100Z25A piezo scanning stage. The scan trajectory covered a 10 μm $\times$ 10 μm area, consisting of 323 scanning points arranged on a series of concentric circles, with a 0.5 μm radial increment between adjacent rings. This scanning pattern has been shown to reduce scanning trajectory artefacts associated with a raster scanning grid [11]. The diffraction dataset was recorded 3.2 m downstream from the test sample using a Timepix photon-counting detector with 55 μm square pixels. 30 images were recorded and summed for each ptychographic scan position. The data acquisition time for each image was 0.04 seconds. Additional ptychographic datasets were recorded using slit widths of 20 μm $\times$ 40 μm and 40 μm $\times$ 50 μm. The remaining experimental parameters were the same as those used in the 10 μm $\times$ 20 μm dataset acquisition. The region of interest in all diffraction data was set to a 256 $\times$ 256 array centred on the diffraction peak. The experimental parameters resulted in a sample plane sampling interval of 31 nm.

4. Results

The sample transmission function and probe were retrieved using the 10 μm $\times$ 20 μm dataset and the standard ePIE algorithm for a total of 500 iterations. The initial estimate for the sample transmission function was a random binary array, with an initial probe estimate based on a knife edge scan of the central lobe. The resulting reconstructed sample transmission phase

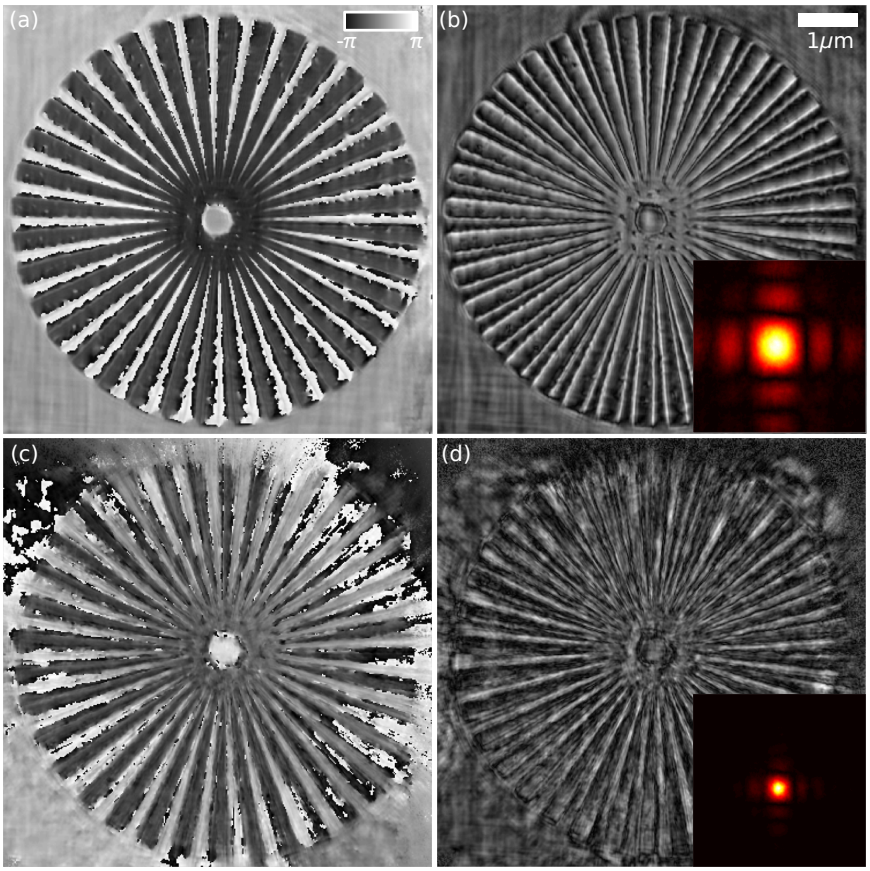

Fig. 2. Retrieved sample transmission phase and amplitude for the 10 μm $\times$ 20 μm dataset using the standard ePIE algorithm are shown in (a) and (b) respectively. The reconstructed probe amplitude is shown in the inset in (a). The corresponding ePIE reconstructions for the 20 μm $\times$ 40 μm dataset are shown in (c) and (d). Scale bars are common.

and amplitude are shown in Fig. 2 (a) and (b) respectively. The retrieved sample transmission phase is presented in phase-wrapped form as the rapid phase transitions introduced subsequent errors in the phase-unwrapping algorithms. The reconstructed probe amplitude is provided in the inset in Fig. 2 (b). Although the reconstructed sample image is qualitatively similar to the SEM image in Fig. 1 (a), the sample transmission phase and amplitude both exhibit a strongly correlated erroneous variation in the lithographed regions, known to be of uniform density. An additional 500 iterations iterations yielded no qualitative improvement in the sample image and no reduction in the χ^2 metric given in Eq. 2. The reconstructions were tested using 10 distinct random binary initial estimates of the sample transmission function. The resulting reconstructions yielded image artefacts that were inconsistent between reconstructions, indicating a local (but not global) minimisation of the χ^2 metric for each reconstruction. The oversampling ratio is given by $\sigma = N/N_s$ [13], where N is the total number of elements of the propagated wavefield (i.e. 256^2) and N_s is the total number of non-zero elements in the exit surface wave, yielding an oversampling ratio of $\sigma = 2.4$. The overlap between adjacent probe positions was 75%.

The sample transmission function and probe were reconstructed using the ePIE algorithm and the 20 μm $\times$ 40 μm dataset. The resulting sample transmission phase and amplitude re-

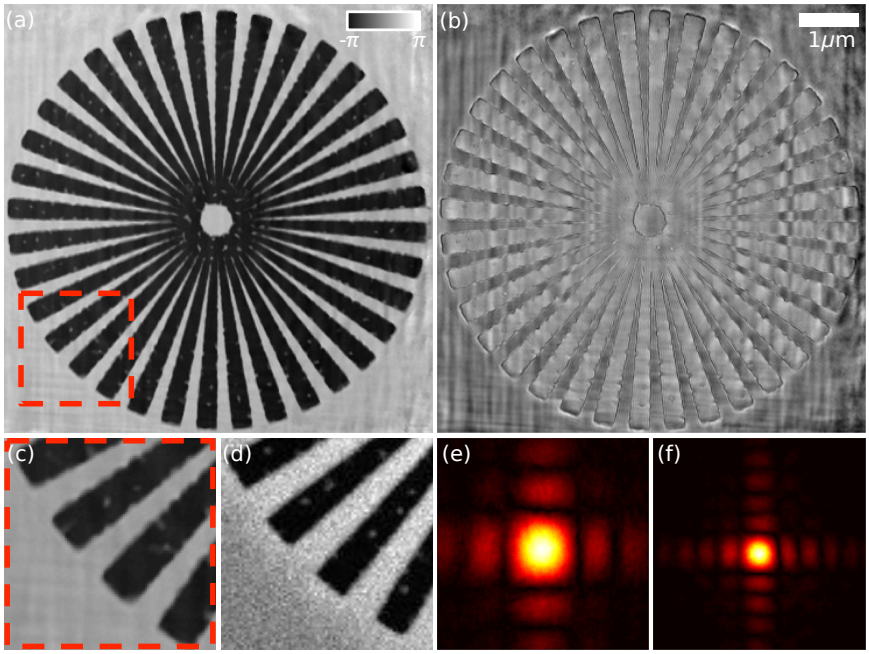

Fig. 3. Probe-diverse ePIE sample phase and amplitude reconstructions using a sparsely distributed dataset constructed from both the 10 μm $\times$ 20 μm and 20 μm $\times$ 40 μm datasets shown in (a) and (b) respectively. The reconstructed probes are shown in (d) and (e).

constructions are provided in Fig. 2 (c) and (d). The retrieved sample transmission phase is presented in phase-wrapped form due to additional errors introduced by the phase unwrapping algorithms. The correlation between erroneous amplitude and phase variation, noted in the 10 μm $\times$ 20 μm sample transmission reconstruction, is also present in the 20 μm $\times$ 40 μm dataset reconstructions. The reconstructed probe amplitude is provided in the inset in Fig. 2 (d). The reduction in reconstruction quality compared to the 10 μm $\times$ 20 μm dataset reconstructions may be largely attributed to the decrease in probe size and corresponding decrease in probe overlap, determined to be 61% between adjacent probe positions. The oversampling ratio for the smaller probe was $\sigma = 6.4$.

The sample transmission function was reconstructed using the probe-diverse ePIE algorithm and a mixed ptychographic dataset consisting of diffraction data recorded at every second point in the scanning trajectory of both the 10 μm $\times$ 20 μm and 20 μm $\times$ 40 μm datasets. This resulted in a mixed diffraction dataset containing 323 diffraction images in total, i.e. a dataset of the same size as the single-probe ePIE reconstructions. The mean overlap ratio for the sparsely distributed dataset was 30% lower than the 10 μm $\times$ 20 μm dataset (i.e. the dataset with a larger probe). An estimate of the sparsely distributed dataset oversampling ratio may be obtained from the average oversampling ratio, i.e. $\sigma = 4.4$.

The remaining algorithm parameters were the same as those used in the standard ePIE reconstructions. The probe-diverse sample transmission phase and amplitude are shown in Fig. 3 (a) and (b). There is a significant improvement in the probe-diverse reconstructed sample image compared to the single-probe reconstructions in Fig 2. In particular the erroneous amplitude and phase variation present in the single-probe reconstructions is almost completely absent in the probe-diverse reconstructions, with a subsequent improvement in the imaging accuracy of the tungsten deposits, shown in closeup in Fig. 3 (c). The distribution of the tungsten deposits

in the SEM image in Fig. 3 (d) indicates that the reconstructed sample image is of a different star (the sample consisted of multiple copies of the star aperture). The reconstructed probe amplitudes are shown in (e) and (f). The improvements in the reconstructed sample image yielded a reduction in the χ^2 metric for all scan positions and a 20% reduction in the mean χ^2 value.

The sample image was then reconstructed using the probe-diverse ePIE algorithm and the entire dataset from both the 10 μm $\times$ 20 μm and 20 μm $\times$ 40 μm datasets (i.e. 626 diffraction images in total). There was no significant improvement in the sample image quality or reduction in the χ^2 metric compared to the sparsely distributed data reconstructions. A final test was performed using additional data from the 40 μm $\times$ 50 μm dataset (i.e. 969 data-points in total), with no significant improvement in the reconstructed sample image compared to the reconstructions obtained with two probes.

5. Conclusion

The proposed algorithm can use ptychographic data obtained by scanning a target sample through multiple distinct probes to obtain high-resolution reconstructions of the sample image. Using a mixed ptychographic dataset of equal size to the standard single-probe reconstructions, the probe-diverse method was shown to yield significant improvements in the sample image compared to those obtained using the standard single-probe ePIE algorithm. These improvements were obtained with no increase in the data acquisition time.

The use of a two-probe ptychographic system appears to have been effective in overcoming the stagnation encountered in the standard single probe scheme and thereby assist in the global optimisation of the sample image retrieval. Additional ptychographic data, whether from data acquired at additional scanning trajectory points in the two-probe system, or from additional data acquired with a third distinct probe, yielded negligible improvement in the probe-diverse sample image reconstructions.

6. Acknowledgments

The measurements were carried out at APS beamline 34-ID-C, built with US National Science Foundation grant DMR-9724294 and operated by the US Department of Energy, Office of Basic Energy Sciences, under contract no. DE-AC0206CH11357. I. Peterson acknowledges support from the Australian Research Council Centre of Excellence for Coherent X-ray Science. I. K. Robinson acknowledges support from the UK EPSRC under EP/I022562/1 “Phase modulation technology for X-ray imaging”.